

Upconversion photoluminescence and optical temperature sensing properties of $\text{PbNb}_2\text{O}_6:\text{Yb}^{3+}, \text{Ln}^{3+}$ ($\text{Ln}^{3+}=\text{Er}^{3+}/\text{Ho}^{3+}$) ceramics

Z. Liu ^{a,*}, K. Li ^b, Y. Sun ^c, R. X. Wang ^a

^a School of Science, Jinling Institute of Technology, Nanjing 211168, China

^b Guangdong Provincial Key Laboratory of Electronic Functional Materials and Devices, Huizhou University, Huizhou 516001, Guangdong, China

^c Precision Acousto-optic Instrument Institute, School of Instrumentation Science and Engineering, Harbin Institute of Technology, Harbin 150080, China

Through conventional solid-state sintering process, $\text{PbNb}_2\text{O}_6:\text{Yb}^{3+}, \text{Ln}^{3+}$ ($\text{Ln}^{3+}=\text{Er}^{3+}/\text{Ho}^{3+}$) ceramics have been fabricated. The structural information of synthesized ceramics was obtained via X-ray diffraction. Scanning electron microscopy was utilized to investigate their morphological properties. The investigation of upconversion photoluminescence properties of the synthesized ceramics was conducted by analyzing upconversion emission spectra upon excitation with 980 nm light. Power dependence studies confirmed the presence of two-photon absorption processes in both $\text{PbNb}_2\text{O}_6:\text{Yb}^{3+}, \text{Er}^{3+}$ and $\text{PbNb}_2\text{O}_6:\text{Yb}^{3+}, \text{Ho}^{3+}$ ceramics. Temperature-dependent experiments from 303 K to 513 K demonstrated significant variations in emission intensities and fluorescence intensity ratios (FIR), enabling the assessment of temperature changes. The absolute sensitivity of PbNb_2O_6 ceramic co-doped with $\text{Yb}^{3+}, \text{Er}^{3+}$ ions reached its maximum value of 0.0056 K^{-1} at 513 K, while the maximum relative sensitivity of $0.697\% \text{ K}^{-1}$ was recorded at 339 K. For PbNb_2O_6 ceramic co-doped with $\text{Yb}^{3+}, \text{Ho}^{3+}$ ions, the maximum values of absolute and relative sensitivities were 0.048 K^{-1} and $0.8\% \text{ K}^{-1}$ at 513 K and 473 K, respectively. These results highlight the potential applications of $\text{PbNb}_2\text{O}_6:\text{Yb}^{3+}, \text{Ln}^{3+}$ ($\text{Ln}^{3+}=\text{Er}^{3+}/\text{Ho}^{3+}$) ceramics in advanced temperature sensing based on photoluminescence.

(Received October 3, 2024; Accepted December 6, 2024)

Keywords: Upconversion, Fluorescence intensity ratio, Temperature sensing, $\text{PbNb}_2\text{O}_6:\text{Yb}^{3+}, \text{Ln}^{3+}$ ($\text{Ln}^{3+}=\text{Er}^{3+}/\text{Ho}^{3+}$), Ceramics

1. Introduction

Science and technology have benefited greatly from luminescent materials, which are used in solid state lasers, phosphor-converted LEDs, solar cells, bio-imaging, anti-counterfeiting, sensing, and photo-catalysis [1-7]. Due to the unique nonlinear spectral conversion properties, upconversion photoluminescence has attracted considerable attention as an anti-stokes process with emission wavelength shorter than excitation wavelength. The process absorbs multiple low-energy photons and emits high-energy photons [8]. Inorganic rare earth luminescent materials

* Corresponding author: liuzhen@jit.edu.cn

<https://doi.org/10.15251/CL.2024.2112.977>

can achieve the upconversion process by rationally design components, which are composed of rare earth activators, sensitizers and inorganic host matrix materials. In past decades, a series of upconversion luminescent materials with rare earth dopants have been developed for investigation on mechanisms of photoluminescence and their various applications [9, 10].

The trivalent lanthanide ions, including Tm^{3+} , Ho^{3+} , Er^{3+} , commonly serve as activator ions for triggering photoluminescence. The upconversion emission spectra arising from these three ions upon appropriate wavelength excitation can cover a wide spectral range, including ultraviolet, visible and infrared light. By incorporating $\text{Tm}^{3+}/\text{Ho}^{3+}/\text{Er}^{3+}$ dopants, Li et al. developed dual perovskite phosphors capable of emitting light in multiple colors [11]. Jia et al. reported the synergistic effects of 980 nm and 1973 nm excitation on tunable visible upconversion emissions from Er^{3+} [12]. Several researchers explored the upconversion emission of varied phosphors codoped with $\text{Er}^{3+}/\text{Tm}^{3+}$ under excitation of near-infrared light [13-15]. Yu et al. achieved ultraviolet emissions in Ho^{3+} activated phosphors by optimizing energy transfer process [16]. Nonetheless, Ho^{3+} cannot be directly excited by 980 nm light. Additionally, the absorption cross-section of 980 nm light for singly doped Er^{3+} is lower than that of the sensitizer, which can transfer energy to Er^{3+} to improve its upconversion emission. Yb^{3+} ions is generally employed as sensitizers for boosting the absorption of 980 nm light.

The upconversion emissions from activated rare-earth ions could exhibit different behaviors as a result of distinct host matrix materials. Meanwhile, the host materials could be in various forms, including nanoparticles, thin films, polycrystalline powders, ceramics and single crystals [17-21]. Among them, functional ceramics as host materials offer several advantages, including low cost, a simple fabrication process, durability, high chemical and thermal stability. Meanwhile, doping them with rare earths facilitates the integration of the intrinsic properties of functional ceramics with the luminescent properties of rare earth ions into a single material. In recent years, researchers have developed many ferroelectric ceramics doped with rare earth ions for exploring various potential applications [22-24]. PbNb_2O_6 is a typical ferroelectric material with high curie temperature. Previously, scientists dedicated substantial attention to improve the electrical and optical properties of PbNb_2O_6 ceramics [25-28]. However, there is no report on the optical temperature sensing performance and upconversion photoluminescence of PbNb_2O_6 based ceramics. To understanding the photoluminescence properties of $\text{Er}^{3+}/\text{Ho}^{3+}$ activated PbNb_2O_6 based ceramics, a systematic investigation is essential.

In present work, $\text{Pb}_{0.975}\text{Yb}_{0.02}\text{Er}_{0.005}\text{Nb}_2\text{O}_6$ and $\text{Pb}_{0.975}\text{Yb}_{0.02}\text{Ho}_{0.005}\text{Nb}_2\text{O}_6$, ceramics were synthesized. The structural features of synthesized ceramics were characterized by X-ray diffraction. Drawing from the upconversion photoluminescence of Er^{3+} and Ho^{3+} ions within synthesized ceramics, the temperature sensing properties of $\text{Er}^{3+}/\text{Ho}^{3+}$ activated PbNb_2O_6 were investigated via fluorescence intensity ratio technique.

2. Experimental procedures

The $\text{Yb}^{3+}/\text{Ln}^{3+}$ ($\text{Ln}=\text{Er}, \text{Ho}$) co-doped PbNb_2O_6 ceramics were fabricated via conventional solid-state reaction method [29]. The raw materials for ceramics manufacturing were PbO , Nb_2O_5 , Yb_2O_3 , Er_2O_3 and Ho_2O_3 without further purification. These raw materials were accurately weighed and mixed according to stoichiometric ratio specified in the designed chemical formulas

of $\text{Pb}_{0.975}\text{Yb}_{0.02}\text{Er}_{0.005}\text{Nb}_2\text{O}_6$ and $\text{Pb}_{0.975}\text{Yb}_{0.02}\text{Ho}_{0.005}\text{Nb}_2\text{O}_6$, respectively. The mixed powders were then ball milled with anhydrous ethanol for 12 h. After milling, the slurry underwent drying in an oven at 90 °C for 3 h to obtain dry mixed reactants. The dry mixtures were subsequently placed into alumina crucible and calcined at 1100 °C in muffle furnace for 2 h, after which they cooled naturally to ambient temperature. After calcination, the powders were thoroughly blended with polyvinyl alcohol binder (PVA, 5%) and compressed into cylindrical pellets with a diameter of 13 mm [30]. Finally, these pellets were subjected to a binder burning-out process at 550 °C for 1 h and high-temperature sintering process at 1260 °C for 2 h to obtain the ceramics.

X-ray diffraction (XRD) patterns of $\text{Pb}_{0.975}\text{Yb}_{0.02}\text{Er}_{0.005}\text{Nb}_2\text{O}_6$ and $\text{Pb}_{0.975}\text{Yb}_{0.02}\text{Ho}_{0.005}\text{Nb}_2\text{O}_6$ ceramics were recorded using X-ray diffractometer [29]. The morphological properties of the synthesized ceramics were characterized via scanning electron microscopy (SEM) [29]. Before the SEM examination, gold was lightly sputtered on the cross-section of ceramic samples for enhancing the electrical conductivity and improving the quality of SEM images. The upconversion photoluminescence of the ceramic samples was excited via a power tunable diode laser ($\lambda = 980$ nm, Power = 0-1 W). The upconversion photoluminescence spectra of these ceramics were collected via a fiber spectrometer with CCD detector (PG2000 Pro, Ideaoptics) [31]. The fiber probe was equipped with 880 nm low-pass filter. For obtaining the temperature sensitive upconversion emission spectra of the synthesized ceramics, the temperature of the samples was controlled by a program-controlled heating stage [31].

3. Results and discussion

In order to investigate the structural properties, XRD patterns of $\text{PbNb}_2\text{O}_6:\text{Yb}^{3+}/\text{Ln}^{3+}$ ($\text{Ln}^{3+}=\text{Er}^{3+}, \text{Ho}^{3+}$) ceramics, specifically for $\text{Pb}_{0.975}\text{Yb}_{0.02}\text{Er}_{0.005}\text{Nb}_2\text{O}_6$ and $\text{Pb}_{0.975}\text{Yb}_{0.02}\text{Ho}_{0.005}\text{Nb}_2\text{O}_6$ were recorded in 2θ range from 10° - 70°, as shown in Fig. 1. The diffraction patterns are matched well with the standard card (JCPDS Card No. 11-012), suggesting the synthesized samples exhibit orthorhombic phase structure. It can be clearly seen that XRD patterns of $\text{Pb}_{0.975}\text{Yb}_{0.02}\text{Er}_{0.005}\text{Nb}_2\text{O}_6$ and $\text{Pb}_{0.975}\text{Yb}_{0.02}\text{Ho}_{0.005}\text{Nb}_2\text{O}_6$ are similar, indicating the host crystal structure were not significantly altered by the incorporation of Yb^{3+} , Er^{3+} and Ho^{3+} . No impure peaks of Er_2O_3 , Ho_2O_3 and Yb_2O_3 appears in the diffraction patterns, indicating the Yb^{3+} , Er^{3+} and Ho^{3+} ions were successfully entered into the lattice of orthorhombic tungsten bronze PbNb_2O_6 host materials as a result of similar ion radii for Er^{3+} (0.89 Å), Ho^{3+} (0.901 Å), Yb^{3+} (0.868 Å) and Pb^{2+} (1.19 Å).

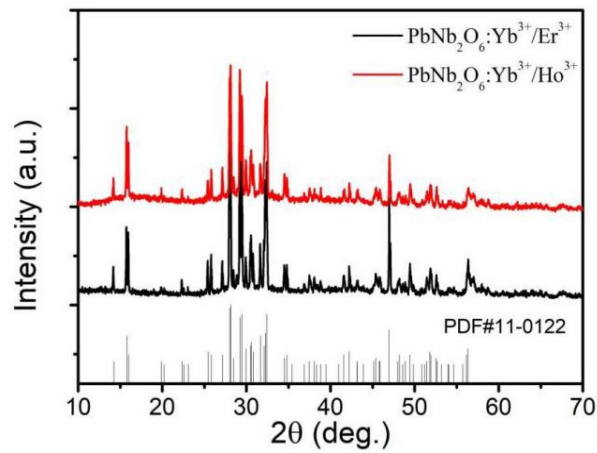


Fig. 1. XRD patterns of $\text{PbNb}_2\text{O}_6:\text{Yb}^{3+}$, Ln^{3+} ($\text{Ln}^{3+}=\text{Er}^{3+}/\text{Ho}^{3+}$) ceramics.

Morphological properties of the synthesized ceramics were investigated by analyzing the cross-sectional SEM images. Fig. 2 (a) and (b) display the SEM images of $\text{Pb}_{0.975}\text{Yb}_{0.02}\text{Er}_{0.005}\text{Nb}_2\text{O}_6$ and $\text{Pb}_{0.975}\text{Yb}_{0.02}\text{Ho}_{0.005}\text{Nb}_2\text{O}_6$ ceramics, respectively. A high density of pores can be found on the grains, which have an irregular shape.

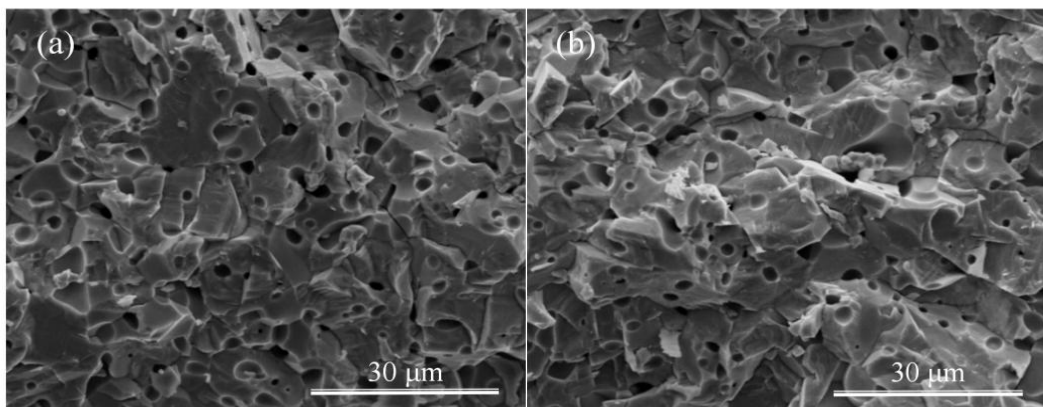


Fig. 2 SEM images of (a) $\text{Pb}_{0.975}\text{Yb}_{0.02}\text{Er}_{0.005}\text{Nb}_2\text{O}_6$, and (b) $\text{Pb}_{0.975}\text{Yb}_{0.02}\text{Ho}_{0.005}\text{Nb}_2\text{O}_6$ ceramics.

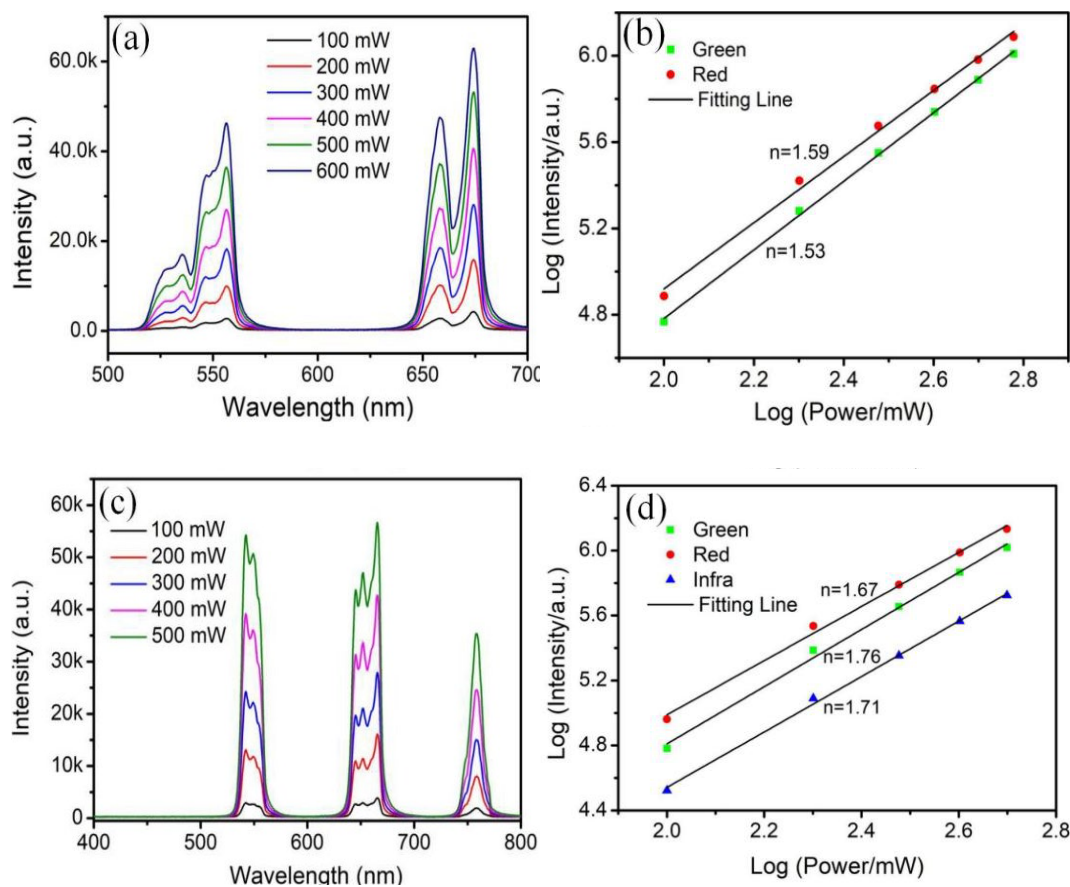


Fig. 3. (a) Pump power dependent upconversion emission spectra, (b) Dual-logarithmic plot of integrated emission intensity against excitation power for $Pb_{0.975}Yb_{0.02}Er_{0.005}Nb_2O_6$ ceramic, (c) Pump power dependence of upconversion emission spectra, (d) Dual-logarithmic plot of integrated emission intensity against excitation power for $Pb_{0.975}Yb_{0.02}Ho_{0.005}Nb_2O_6$ ceramic.

For elucidating the mechanism of upconversion excitation for Yb^{3+} , Er^{3+} and Yb^{3+} , Ho^{3+} ion pairs in $PbNb_2O_6$ matrix, excitation power dependence of upconversion emission has been investigated. Fig. 3(a), (c) depict the pump power dependent upconversion emission spectra of $Pb_{0.975}Yb_{0.02}Er_{0.005}Nb_2O_6$ and $Pb_{0.975}Yb_{0.02}Ho_{0.005}Nb_2O_6$ ceramics, respectively. As shown in Fig. 3(a), the upconversion emission spectra for $Pb_{0.975}Yb_{0.02}Er_{0.005}Nb_2O_6$ exhibit significant emission bands within spectral ranges of 510-580 nm and 638-700 nm, which can be attributed to ${}^2H_{11/2}$, ${}^4S_{3/2} \rightarrow {}^4I_{15/2}$ and ${}^2F_{9/2} \rightarrow {}^4I_{15/2}$ transitions of Er^{3+} ions, respectively [32]. The splitting emission peaks are involved in red emission band, which can be attributed to the Stark splitting of ${}^2F_{9/2}$ energy level. With the increasing of pump power from 100 to 600 mW, the intensities for both green and red emission bands of $Pb_{0.975}Yb_{0.02}Er_{0.005}Nb_2O_6$ ceramic are significantly enhanced, suggesting the upconversion emission is closely related to excitation power. As depicted in Fig. 3(c), the upconversion emission spectra for the $Pb_{0.975}Yb_{0.02}Ho_{0.005}Nb_2O_6$ ceramic show three distinct emission bands between 400 nm and 800 nm. These bands include a green emission peaking at 542 nm, a red emission at 665 nm, and an infrared emission at 757 nm, which are associated with the 5F_4 , ${}^5S_2 \rightarrow {}^5I_8$, ${}^5F_5 \rightarrow {}^5I_8$ and 5F_4 , ${}^5S_2 \rightarrow {}^5I_6$ transitions of Ho^{3+} ions, respectively [33]. As the excitation

power is raised from 100 mW to 500 mW, the intensities of green, red and infrared emissions for $\text{Pb}_{0.975}\text{Yb}_{0.02}\text{Ho}_{0.005}\text{Nb}_2\text{O}_6$ ceramic increase monotonically.

For unsaturated excitation regime, the excitation power dependence of integral emission intensity can be analyzed through the following formula (1) [34].

$$I \propto P_{\text{exc}}^n \quad (1)$$

Herein, I represents the integral upconversion emission intensity, P_{exc} denotes the excitation power of incident light, and the index n indicates quantity of photons that participate in the process of upconversion excitation through absorption [34]. To clarify the quantity of photons participating in the upconversion process for the synthesized $\text{Pb}_{0.975}\text{Yb}_{0.02}\text{Er}_{0.005}\text{Nb}_2\text{O}_6$ and $\text{Pb}_{0.975}\text{Yb}_{0.02}\text{Ho}_{0.005}\text{Nb}_2\text{O}_6$ ceramics, the logarithmic values of integral emission intensities against that of excitation powers of 980 nm laser are investigated, respectively. As illustrated in Fig. 3 (b), the logarithmic integral emission intensities for both green and red emission bands versus logarithmic pump power can be linearly fitted, as described in formula (1). According to the fitting results, the slopes for green and red emission bands are 1.53 and 1.59, respectively. It suggests that the upconversion photoluminescence of $\text{Pb}_{0.975}\text{Yb}_{0.02}\text{Er}_{0.005}\text{Nb}_2\text{O}_6$ ceramic, when excited by 980 nm light, is associated with the absorption of two photons. Fig. 3 (d) shows dual-logarithmic plot for the emission intensities of three emission bands for $\text{Pb}_{0.975}\text{Yb}_{0.02}\text{Ho}_{0.005}\text{Nb}_2\text{O}_6$ ceramic and pump power. A linear function can also be used to fit the experimental data, with slopes of 1.76 for green, 1.67 for red and 1.71 for infrared emission bands. All the slopes are close to 2, indicating the two photons absorption is dominant for excitation of upconversion photoluminescence of $\text{Pb}_{0.975}\text{Yb}_{0.02}\text{Ho}_{0.005}\text{Nb}_2\text{O}_6$ ceramic.

In order to explore the potential applications of $\text{Pb}_{0.975}\text{Yb}_{0.02}\text{Er}_{0.005}\text{Nb}_2\text{O}_6$ and $\text{Pb}_{0.975}\text{Yb}_{0.02}\text{Ho}_{0.005}\text{Nb}_2\text{O}_6$ ceramics for luminescence thermometry, their temperature dependent upconversion emission spectra were recorded within temperature range of 303-513 K. The 980 nm light excited upconversion emission spectra of $\text{Pb}_{0.975}\text{Yb}_{0.02}\text{Er}_{0.005}\text{Nb}_2\text{O}_6$ ceramic at different temperatures are depicted in Fig. 4 (a). As shown, the emission intensity changes significantly with increasing of temperature. The temperature-sensitive integral intensities of the ${}^2\text{H}_{11/2}$, ${}^4\text{S}_{3/2} \rightarrow {}^4\text{I}_{15/2}$ (abbreviated as G1, G2) and ${}^2\text{F}_{9/2}^{(1,2)} \rightarrow {}^4\text{I}_{15/2}$ (abbreviated as R1, R2) transitions are illustrated in Fig. 4 (b). As shown, the intensity of G2 emission monotonically decreases with elevation of temperature, which is a classical phenomenon of thermal quenching. However, the emission intensities for G1, R1 and R2 bands initially increase with temperature and then decrease. The different trends can be associated with the thermal excitation of thermal coupled energy levels and thermal enhanced non-radiative relaxation.

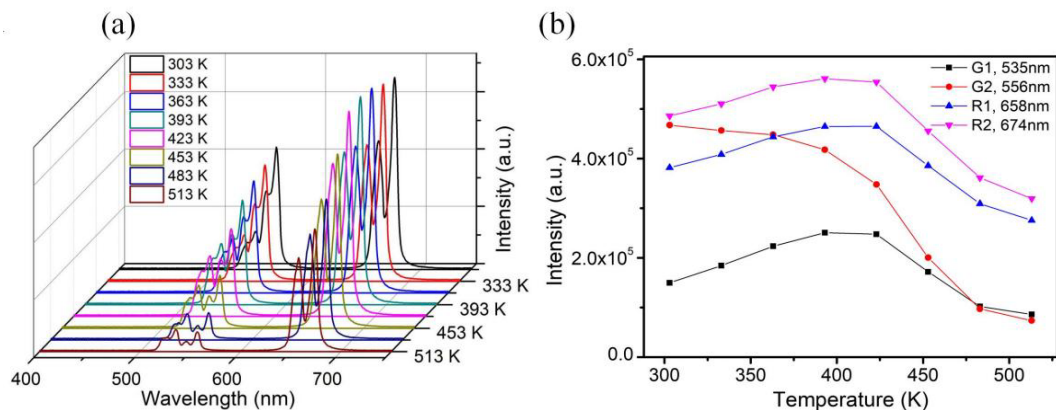


Fig. 4. (a) Upconversion emission spectra of $Pb_{0.975}Yb_{0.02}Er_{0.005}Nb_2O_6$ ceramic at different temperature, (b) Integral intensities of the G1, G2, R1 and R2 emission sub-bands as a function of temperature.

For optical thermometry applications, the temperature-sensitive fluorescence intensity ratio (FIR) can generally be described by the following equation (2) [35],

$$FIR = A \exp(B/T) + C \quad (2)$$

where, T represents the absolute temperature, A, B and C are constants.

Temperature-dependent sensitivities, including absolute sensitivity (abbreviated as S_a) and relative sensitivity (abbreviated as S_r), are critical indices for assessing the performance of temperature sensors [35]. The S_a and S_r for FIR based optical temperature sensing can be calculated as follow equations (3) and (4), respectively.

$$S_a = \left| \frac{dFIR}{dT} \right| \quad (3)$$

$$S_r = \frac{1}{FIR} \left| \frac{dFIR}{dT} \right| \times 100\% \quad (4)$$

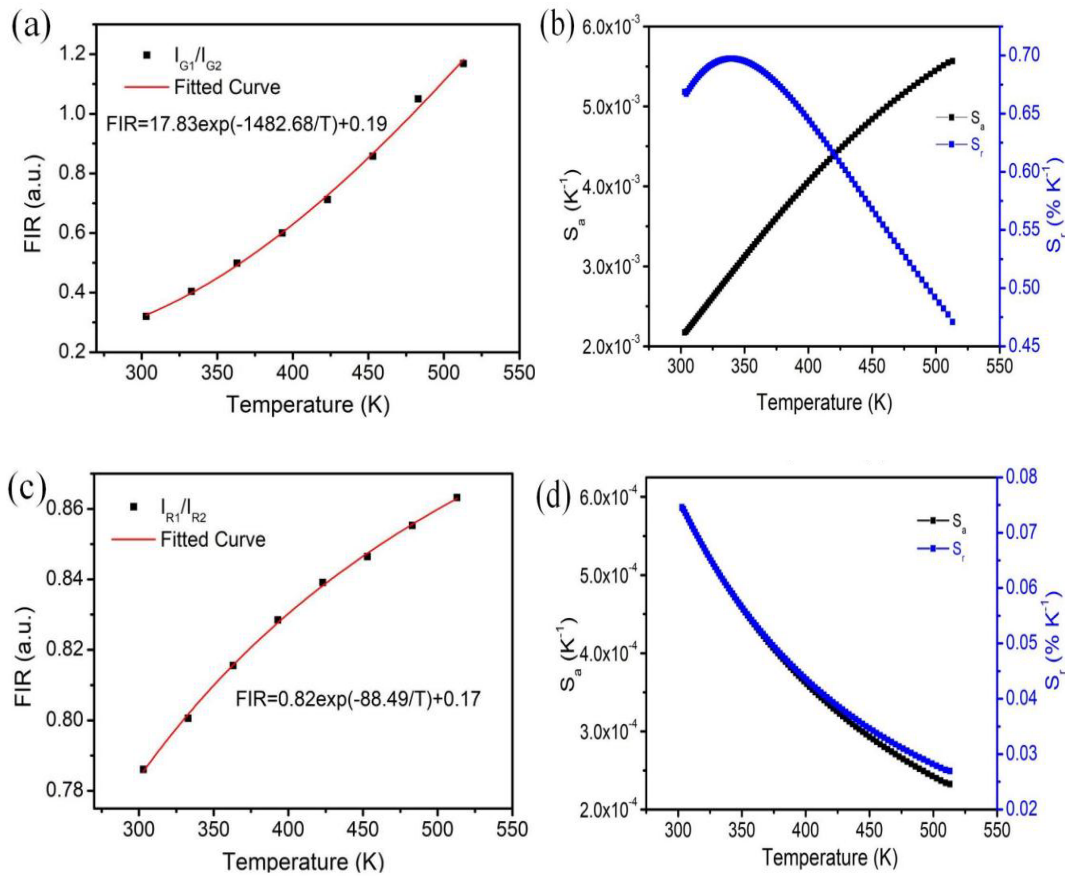


Fig. 5. (a) Temperature-dependent FIR (I_{G1}/I_{G2}), (b) Temperature dependence of S_a and S_r , derived from I_{G1}/I_{G2} of $\text{Pb}_{0.975}\text{Yb}_{0.02}\text{Er}_{0.005}\text{Nb}_2\text{O}_6$ ceramic, (c) Temperature-dependent FIR (I_{R1}/I_{R2}), (d) Temperature dependence of S_a and S_r , derived from I_{R1}/I_{R2} of $\text{Pb}_{0.975}\text{Yb}_{0.02}\text{Er}_{0.005}\text{Nb}_2\text{O}_6$ ceramic.

The FIR method was utilized to analyze the optical temperature-sensitive photoluminescence properties of $\text{Pb}_{0.975}\text{Yb}_{0.02}\text{Er}_{0.005}\text{Nb}_2\text{O}_6$ ceramic. Fig. 5 (a) and (c) display the temperature-dependent FIR based on I_{G1}/I_{G2} and I_{R1}/I_{R2} , respectively. As shown, the temperature-dependent FIR can be well fitted by equation (2). The fitted results show the values of A, B, and C constants for I_{G1}/I_{G2} of $\text{Pb}_{0.975}\text{Yb}_{0.02}\text{Er}_{0.005}\text{Nb}_2\text{O}_6$ are 17.83, -1482.68 and 0.19, respectively. For I_{R1}/I_{R2} of $\text{Pb}_{0.975}\text{Yb}_{0.02}\text{Er}_{0.005}\text{Nb}_2\text{O}_6$, the constants are 0.82, -88.49 and 0.17. The temperature-dependent sensitivity curves for S_a and S_r are determined based on equations (3) and (4), respectively. Fig. 5 (b) depicts the temperature dependence of S_a and S_r , derived from I_{G1}/I_{G2} of $\text{Pb}_{0.975}\text{Yb}_{0.02}\text{Er}_{0.005}\text{Nb}_2\text{O}_6$ ceramic. As shown, for I_{G1}/I_{G2} , S_a increases monotonically with increasing temperature from 303 K to 513 K, reaching its maximum value of 0.0056 K⁻¹ at 513 K. The maximum value of S_r is 0.697% K⁻¹ at 339 K. Fig. 5 (d) illustrates the temperature-dependent S_a and S_r , derived from I_{R1}/I_{R2} of $\text{Pb}_{0.975}\text{Yb}_{0.02}\text{Er}_{0.005}\text{Nb}_2\text{O}_6$ ceramic. As illustrated, for I_{R1}/I_{R2} , both S_a and S_r decrease monotonically with the elevation of temperature from 303 K to 513 K, having maximum values of 0.0006 K⁻¹ and 0.075% K⁻¹ at 303 K, respectively.

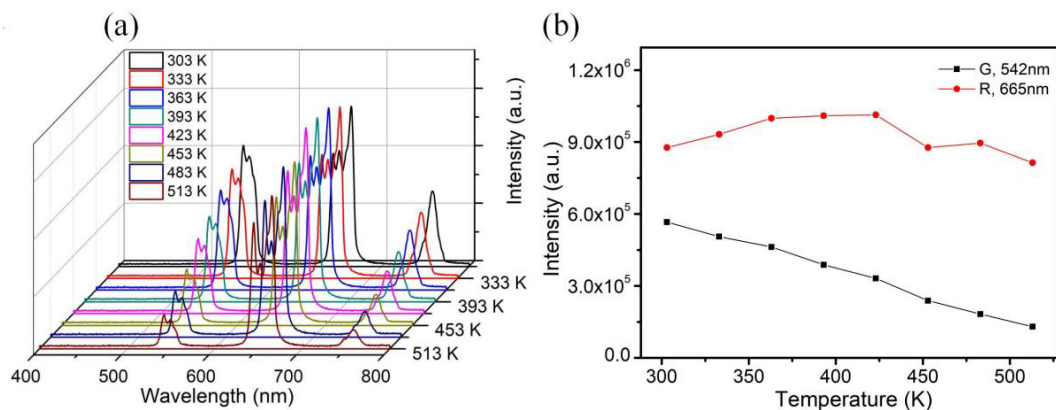


Fig. 6. (a) Upconversion emission spectra of $Pb_{0.975}Yb_{0.02}Ho_{0.005}Nb_2O_6$ ceramic at different temperature, (b) Integral intensities of the G, R emission bands as a function of temperature.

Fig. 6 (a) depicts the upconversion emission spectra of $Pb_{0.975}Yb_{0.02}Ho_{0.005}Nb_2O_6$ ceramic at different temperature. As shown, upon 980 nm light excitation, the spectral shape changes significantly with increasing of temperature. Fig. 6 (b) illustrates the curves of temperature-sensitive integral intensities of the ${}^5F_4, {}^5S_2 \rightarrow {}^5I_8$ (G) transition and ${}^5F_5 \rightarrow {}^5I_8$ (R) transition. It can be seen that the integral intensities of the G and R emission bands change with temperature, exhibiting markedly different trends.

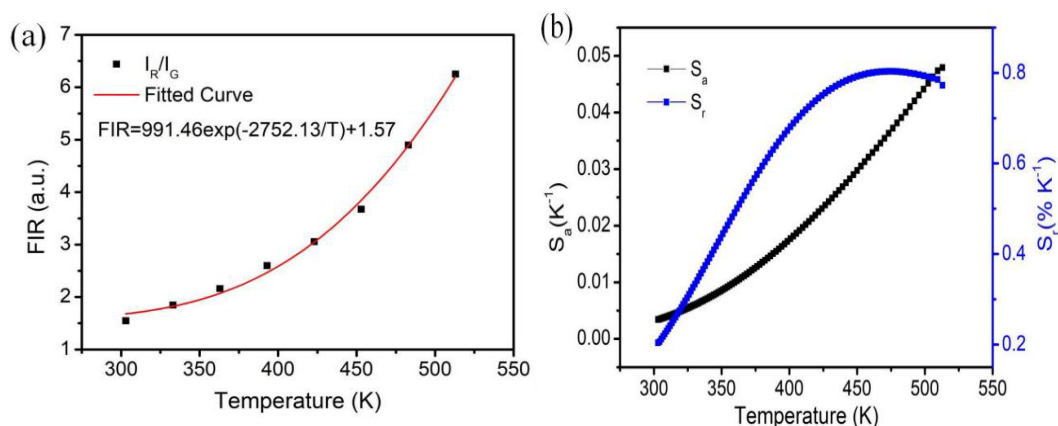


Fig. 7. (a) Temperature-dependent FIR (I_R/I_G), (b) Temperature dependence of S_a and S_r , derived from I_R/I_G of $Pb_{0.975}Yb_{0.02}Ho_{0.005}Nb_2O_6$ ceramic.

The temperature-dependent FIR (I_R/I_G) is depicted in Fig. 7 (a). As displayed, the experimental data of FIR (I_R/I_G) can also be fitted by the equation (2). According to the fitted curve, the A, B and C constants in equation (2) are 991.46, -2752.13 and 1.57. Fig. 7 (b) illustrates the temperature dependence of S_a and S_r , derived from I_R/I_G of $Pb_{0.975}Yb_{0.02}Ho_{0.005}Nb_2O_6$ ceramic. In this scenario, S_a has its maximum values of 0.048 K^{-1} at 513 K, while S_r attains the peak value of $0.8\% \text{ K}^{-1}$ at 473 K.

4. Conclusion

In summary, this study investigates the structural and luminescent properties of synthesized $\text{Pb}_{0.975}\text{Yb}_{0.02}\text{Er}_{0.005}\text{Nb}_2\text{O}_6$ and $\text{Pb}_{0.975}\text{Yb}_{0.02}\text{Ho}_{0.005}\text{Nb}_2\text{O}_6$, ceramics. X-ray diffraction (XRD) analysis confirms their orthorhombic phase structure, with no impurities, suggesting successful incorporation of activator ions into the PbNb_2O_6 lattice. Scanning electron microscopy (SEM) reveals irregularly shaped grains with a high density of pores. The upconversion emission spectra indicate strong green and red emissions for Er^{3+} and three distinct emission bands for Ho^{3+} in PbNb_2O_6 . Power dependence analyses show that upconversion processes involve the absorption of two photons for both ceramics, as indicated by the slopes of logarithmic plots for integrated emission intensity and power. Furthermore, temperature-dependent experiments from 303 K to 513 K reveal significant variations in emission intensity, highlighting the potential of these ceramics for optical thermometry. The temperature sensitivity calculated from fluorescence intensity ratio based optical thermometry demonstrate the applicability of $\text{Pb}_{0.975}\text{Yb}_{0.02}\text{Er}_{0.005}\text{Nb}_2\text{O}_6$ and $\text{Pb}_{0.975}\text{Yb}_{0.02}\text{Ho}_{0.005}\text{Nb}_2\text{O}_6$ in advanced temperature sensing applications.

Acknowledgements

This work is financially supported by Guangdong Provincial Key Laboratory of Electronic Functional Materials and Devices (EFMD2024012M), Jiangsu Provincial Double Innovation Plan (JSSCBS20210616), Research Start-up Program (jit-b-202054), Jiangsu Provincial Natural Science Foundation (BK20201111).

References

- [1] X. Y. Zheng, H. Xie, T. Y. Zhou et al., *Optics Express* 32, 18352 (2024); <https://doi.org/10.1364/OE.518804>
- [2] X, Y. Liu, H. M. Cheng, B. Yue et al., *Journal of Colloid and Interface Science* 666, 162-175 (2024); <https://doi.org/10.1016/j.jcis.2024.04.028>
- [3] S. Fuentes, M. Vega, M. Arias et al., *Materials Letters* 296, 129889 (2021); <https://doi.org/10.1016/j.matlet.2021.129889>
- [4] Y. L. Chang, H. R. Chen, X. Y. Xie et al., *Nature Communications* 14 1079 (2023);
- [5] X. N. Wang, T. Li, W. C. Liang et al., *Journal of the American Ceramic Society* 00, 1-11 (2021)
- [6] Z. H. Ni, Y. Y. Zhu, H. Z. Zhang et al., *Journal of Luminescence* 268, 120427 (2024); <https://doi.org/10.1016/j.jlumin.2023.120427>
- [7] E. Pavitra, L. Antony, K. S. Ranjith et al., *Journal of Alloys and Compounds* 979, 173574 (2024); <https://doi.org/10.1016/j.jallcom.2024.173574>
- [8] X. L. Yan, Y. Z. Cao, T. S. Liu, *Ceramics International* 50, 33995 (2024); <https://doi.org/10.1016/j.ceramint.2024.06.219>

- [9] C. Cascales, C. L. Paina, E. Bazan et al., *Nanotechnology* 28, 185101 (2017); <https://doi.org/10.1088/1361-6528/aa6834>
- [10] G. Nalupurackal, J. Singh, S. Roy et al., *Optics Express* 131, 112695 (2022);
- [11] Y. Fu, X. J. Wang, S. Liu, et al., *Ceramics International* 49, 9547-9583 (2023); <https://doi.org/10.1016/j.ceramint.2022.11.127>
- [12] H. Jia, N. Li, H. Y. He, et al., *Advanced Optical Materials*, 12, 2302583 (2024); <https://doi.org/10.1002/adom.202302583>
- [13] B. Gunay, E. Sariyar, U. Unal, et al., *Colloids and Surfaces A: Physicochemical and Engineering Aspects*, 612, 126003 (2021); <https://doi.org/10.1016/j.colsurfa.2020.126003>
- [14] H. Y. Liu, J. B. Li, P. F. Hu, et al., *Journal of Rare Earths*, 40, 11-19 (2022); <https://doi.org/10.1016/j.jre.2020.11.006>
- [15] T. Grzyb, I. R. Martín, R. Popescu, *Nanoscale*, 16, 1692 (2024); <https://doi.org/10.1039/D3NR04418A>
- [16] Y. Yu, Y. Z. Li, *Journal of Luminescence*, 243, 118619 (2022); <https://doi.org/10.1016/j.jlumin.2021.118671>
- [17] W. Y. Ge, J. D. Shi, M. M. Xu et al., *Journal of Alloys and Compounds* 788, 993-999 (2019); <https://doi.org/10.1016/j.jallcom.2019.02.319>
- [18] E. Hasabeldaim, H. C. Swart, R. E. Kroon, *Physica B: Condensed Matter* 671, 415417 (2023); <https://doi.org/10.1016/j.physb.2023.415417>
- [19] T. Luo, Y. J. Sun, R. N. Wang et al., *Applied Physics Letter* 124, 031102 (2024);
- [20] Y. Huan, C. X. Li, L. Z. Wu et al., *Ceramics International* 50, 16207-16214 (2024); <https://doi.org/10.1016/j.ceramint.2024.02.101>
- [21] Y. Q. Zou, Y. Wang, Z. J. Zhu et al., *Journal of Luminescence* 263, 120037 (2023); <https://doi.org/10.1016/j.jlumin.2023.120037>
- [22] A. Banwal, R. Bokolia, *Ceramics International* 48, 2230-2240 (2022) <https://doi.org/10.1016/j.ceramint.2021.09.314>
- [23] T. Zheng, L.H. Luo, P. Du et al., *Journal of the European Ceramic Society* 38, 575-583 (2018); <https://doi.org/10.1016/j.jeurceramsoc.2017.09.035>
- [24] J. Q. Bi, T. Wei, L. H. Shen et al., *Journal of the American Ceramic Society* 104, 1785-1796 (2021); <https://doi.org/10.1111/jace.17597>
- [25] X. M. Zhao, C. Liu, D. N. Zhang et al., *Ceramics International* 48, 35461-35466 (2022); <https://doi.org/10.1016/j.ceramint.2022.08.149>
- [26] R. R. Fang, Z. Y. Zhou, R. H. Liang et al., *Ceramics International* 47, 26942-26946 (2021); <https://doi.org/10.1016/j.ceramint.2021.06.106>
- [27] M. Ilhan, M. K. Ekmekci, A. Demir, et al., *Journal of Fluorescence* 26, 1637-1643 (2016); <https://doi.org/10.1007/s10895-016-1849-5>
- [28] M. Ilhan, I.C. Keskin, *Physica B: Condensed Matter* 585, 412106 (2020) <https://doi.org/10.1016/j.physb.2020.412106>
- [29] J. Wu, Y. F. Chang, B. Yang et al., *Journal of Materials Science: Materials in Electronics* 42, 7223-7229 (2016)

- [30] Z. Liu, R. X. Wang, D. H. Chen et al., *Journal of Materials Science: Materials in Electronics* 33, 3748-3756 (2022); <https://doi.org/10.1007/s10854-021-07566-y>
- [31] Z. Liu, R. X. Wang, K. W. Sun et al., *Chalcogenide Letters* 20, 439-447 (2023); <https://doi.org/10.15251/CL.2023.207.439>
- [32] Z. Liu, D. H. Chen, *Journal of Alloys and Compounds* 815, 152092 (2020); <https://doi.org/10.1016/j.jallcom.2019.152092>
- [33] Z. Liu, G. C. Jiang, R. X. Wang et al., *Ceramics International* 42, 11309-11313 (2016); <https://doi.org/10.1016/j.ceramint.2016.04.049>
- [34] Z. Antic, V. Lojpur, M. G. Nikoic et al., *Journal of Luminescence* 145, 466-472 (2013); <https://doi.org/10.1016/j.jlumin.2013.08.007>
- [35] K. Pavani, J. P. C. do Nascimento, S.K. Jakka et al., *Journal of Luminescence* 235, 117992 (2021); <https://doi.org/10.1016/j.jlumin.2021.117992>